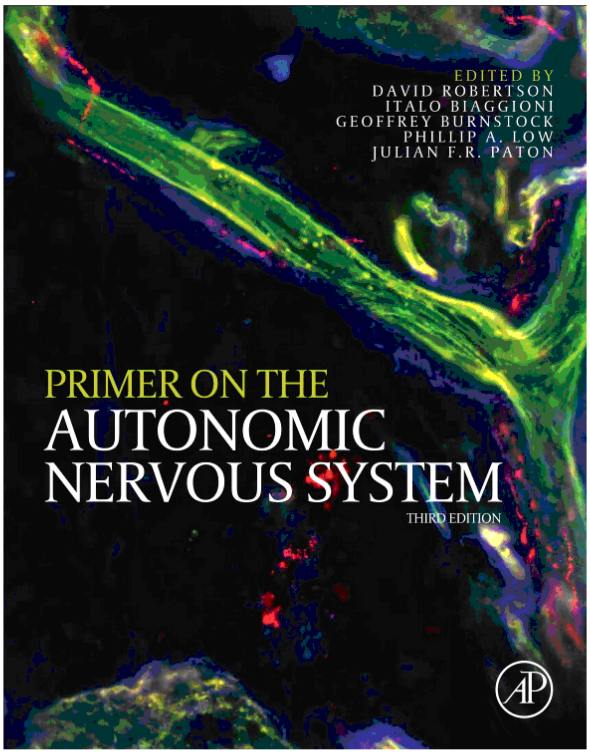




Ilya Rybak, Yaroslav I. Molkov, Julian F. R. Paton, Ana P. L. Abdala and Daniel B. Zoccal, Modeling the Autonomic Nervous System. In: David Robertson, Italo Biaggioni, Geoffrey Burnstock, Phillip A. Low and Julian F.R. Paton, editors, Primer on the Autonomic Nervous System. Oxford: Academic Press, 2012, pp. 681-688.
ISBN: 978-0-12-386525-0

CHAPTER

# 143

# Modeling the Autonomic Nervous System

*Ilya A. Rybak, Yaroslav I. Molkov, Julian F.R. Paton, Ana P.L. Abdala, Daniel B. Zoccal*

Sympathetic nerve activity normally exhibits respiratory modulation that suggests the existence of central interactions between the respiratory and sympathetic networks within the brainstem. A large-scale computational model of interacting respiratory and sympathetic circuits has been developed and used to investigate the possible mechanisms of sympatho-respiratory interactions and their role in the baroreceptor reflex control of sympathetic activity and in the elevated sympathetic activity following chronic intermittent hypoxia. Several model predictions have been formulated and tested experimentally. The model provides important insights into the role of sympatho-respiratory interactions in the control of sympathetic outflow and arterial blood pressure under different physiological and patho-physiological conditions.

## LARGE-SCALE COMPUTATIONAL MODEL OF THE BRAINSTEM SYMPATHO-RESPIRATORY NETWORK

A large-scale computational model of the brainstem sympatho-respiratory network has been developed to simulate the respiratory and sympathetic neural circuits interacting within the brainstem (Fig. 143.1A). The major circuits critically involved in generation of the respiratory rhythm and pattern are located in the ventral respiratory column (VRC) and include (rostral-to-caudal) the Bötzinger (BötC) and pre-Bötzinger (pre-BötC) complexes and the rostral (rVRG) and caudal (cVRG) ventral respiratory groups [1,2]. The core of the respiratory central pattern generator was proposed to include (i) an excitatory pre-inspiratory/inspiratory (pre-I/I) population of neurons with intrinsic bursting properties located in the pre-BötC and (ii) a ring of three mutually inhibiting neural populations: the post-inspiratory (post-I) and augmenting-expiratory (aug-E) populations of BötC, and the early-inspiratory (early-I(1)) population of pre-BötC (Fig. 143.1A, see [2,3]). The respiratory circuitry in the model also incorporates two neural populations within the rVRG, the bulbospinal ramp-inspiratory (ramp-I) neurons, projecting to phrenic motoneurons in the spinal cord that send their axons to the phrenic nerve (PN), and the inhibitory early-I(2) neurons shaping the firing pattern of ramp-I neurons, and a population of bulbospinal premotor expiratory neurons of cVRG (bs-E) projecting to the abdominal motoneurons that define activity of the abdominal nerve (AbN) (Fig. 143.1A).

The sympathetic circuits in the model include neurons located in the rostral (RVLM) and caudal (CVLM) ventrolateral medulla (VLM). Specifically, the RVLM neurons define the activity in the thoracic sympathetic nerve (tSN). In addition, the following populations were included in the model: two populations of 2$^{nd}$ order baroreceptor neurons in the nucleus tractus *solitarii* (NTS) receiving baroreceptor afferents and a population of phase-spanning inspiratory-expiratory neurons (IE) in the ventrolateral pons. (Fig. 143.1A, see also [4]).

The model also incorporates a compartment known as the retrotrapezoid nucleus/parafacial respiratory group (RTN/pFRG), containing neurons performing central chemoreceptor function whose activity is sensitive to $CO_2$. This compartment includes a population of neurons with intrinsic bursting properties termed the late-expiratory (late-E) population (Fig. 143.1A). The inclusion of this population in the RTN/pFRG is based on the multiple experimental data that the late-E activity emerging in AbN during hypercapnia originates in this region [3,5]. In addition to multiple mutual interactions all respiratory neural populations in the model receive excitatory drives from the pons, RTN/pFRG and raphé [2,3].

## MODELING THE EFFECTS OF BARORECEPTOR ACTIVATION ON THE RESPIRATORY PATTERN: INSIGHTS INTO RESPIRATORY–SYMPATHETIC INTERACTIONS

The baroreceptor reflex is an important negative feedback mechanism controlling sympathetic outflow. The classical baroreflex controls tSN via 2$^{nd}$ order barosensitive neurons in the NTS that receive the direct excitatory inputs from baroreceptor afferents. It is suggested that excitatory NTS neurons project to CVLM neurons, which

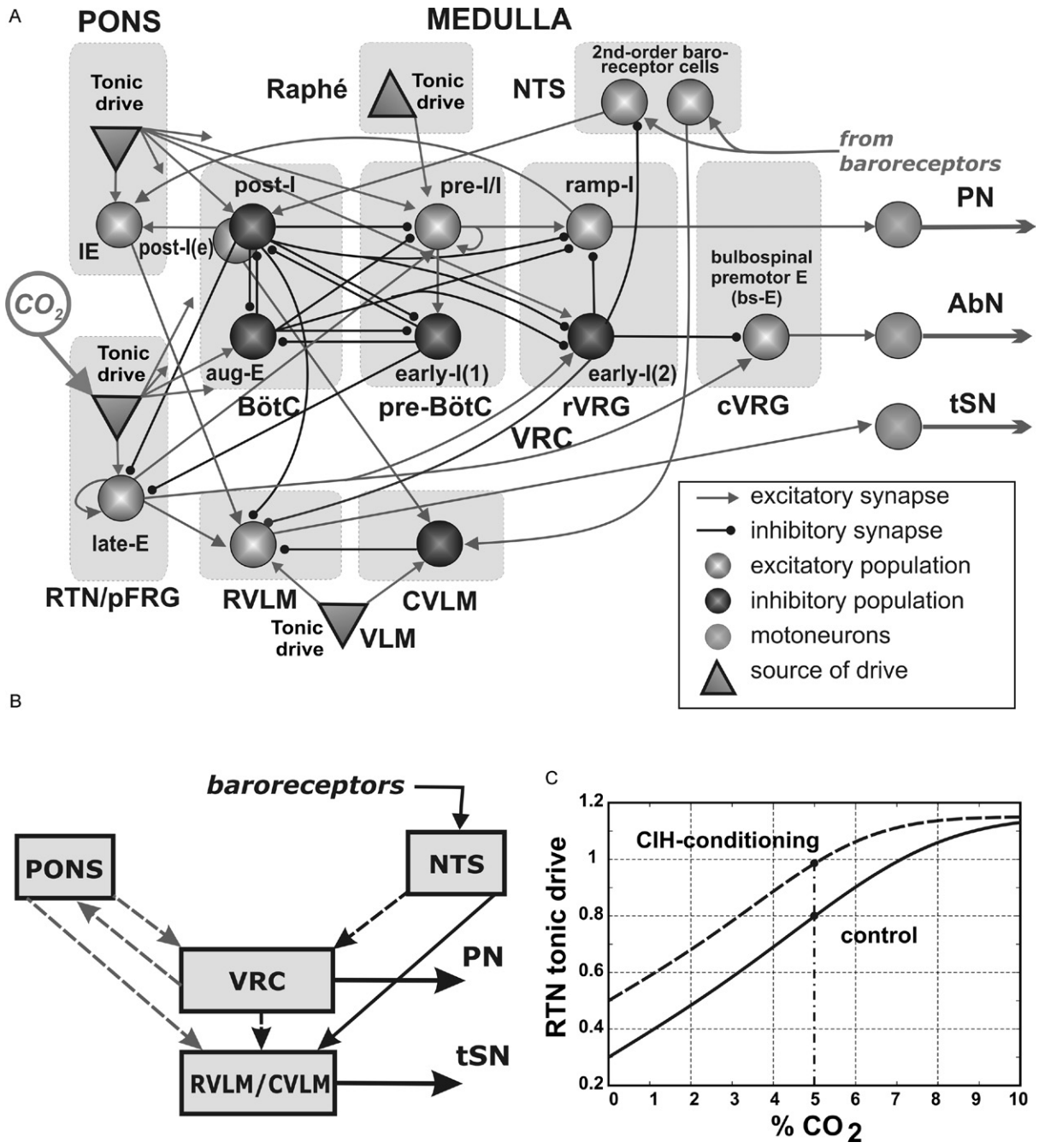


**FIGURE 143.1** The computational model of sympatho-respiratory brainstem network. (A) Schematic of the model showing interactions between different populations of respiratory neurons within major brainstem compartments involved in the control of breathing and sympathetic activity. Abbreviations: *brainstem compartments:* BötC – Bötzinger complex; CVLM – caudal ventrolateral medulla; cVRG – caudal ventral respiratory group; NTS – nucleus tractus solitarii; pre-BötC – pre-Bötzinger complex; RTN/pFRG – retrotrapezoid nucleus/parafacial respiratory group; RVLM – rostral ventrolateral medulla; rVRG – rostral ventral respiratory group; VLM – ventrolateral medulla; VRC – ventral respiratory column; *neural populations:* aug-E – augmenting expiratory; early-I – early-inspiratory; IE – phase-spanning inspiratory-expiratory; late-E – late-expiratory; post-I – post-inspiratory; post-I(e) – post-inspiratory (excitatory); pre-I/I – pre-inspiratory/inspiratory; ramp-I – ramp-inspiratory; *motor outputs:* PN – phrenic nerve; AbN – abdominal nerve; tSN – thoracic sympathetic nerve. Keys are shown in the right-bottom corner. Each population (large sphere) consists of 20–50 neurons modeled in the Hodgkin–Huxley style. All tonic drive sources (gray triangles) provide constant drive, except for RTN/pFRG which is $CO_2$-dependent (see panel C). Not all connections from pontine and RTN/pFRG drive sources are shown. For details see [2,3]. (B) Conceptual model of interaction between VRC, PONS, NTS, and RVLM/CVLM. The sympathetic baroreceptor reflex operates via two pathways: one direct pathway (black solid arrows) includes baroreceptors, NTS ($2^{nd}$ order barosensitive cells) and CVLM, which inhibits RVLM and tSN; the other pathway goes from baroreceptors through NTS and VRC (black dashed arrows), whose post-inspiratory neurons inhibit RVLM and tSN. Gray dashed arrows show interactions between PONS and medullary compartments VRC and RVLM/CVLM. (C) RTN/pFRG tonic drive as function of $CO_2$ for the control (solid curve) and CIH-conditioning (dashed curve) cases.

inhibit RVLM neurons hence lowering the tSN activity (Fig. 143.1B). On the other hand, tSN has an obvious respiratory modulation that persists after vagotomy and decerebration, supporting the idea of central coupling between respiratory and sympathetic networks. In turn, the respiratory activity is known to be modulated by baroreceptor afferents through the same 2nd order barosensitive neurons of NTS. This suggests that central sympathorespiratory interactions may contribute to the dynamic control of sympathetic activity. Specifically, it has been hypothesized [4] that the sympathetic baroreceptor reflex has two major pathways (Fig. 143.1B): one direct path mentioned above, that is independent of the respiratory-sympathetic interactions, and the other, operating via the baroreceptor modulation of the respiratory activity and respiratory-sympathetic interactions and hence dependent on the respiratory modulation of tSN activity.

At rest, the tSN activity typically exhibits a well expressed positive modulation during inspiration and a negative modulation during post-inspiration (see Fig. 143.2A1–A3 before applied stimulations). The tSN respiratory modulation was significantly suppressed or eliminated after removal of the pons, when phrenic nerve (PN) activity transformed to an apneustic pattern with prolonged inspiratory bursts and shortened expiration durations (see Fig. 143.2A4 before applied stimulation), underlying a critical role of the pons in the tSN respiratory modulation [6].

In Figure 143.2A1–A5, the transient increases in the arterial pressure were induced in the arterially perfused *in situ* rat preparation [6]. Stimuli were delivered during inspiration, post-inspiration or late expiration and produced phase-dependent effects on both the phrenic nerve (PN) activity and the respiratory modulation of tSN (Fig. 143.2A1–A3). With pons intact, the applied barostimulation had almost no effect on the amplitude and duration of the phrenic bursts even when stimuli were delivered during inspiration (Fig. 143.2A1). At the same time, these stimuli suppressed or abolished inspiratory modulation of tSN activity. In contrast, the same stimuli delivered during post-inspiration (Fig. 143.2A2) or late expiration (Fig. 143.2A3) produced an increase in the expiration period and decreased the tSN activity. The barostimulation-evoked prolongation of expiration was greater if stimulation was applied later during the expiratory phase (compare Figs 143.2A2 and A3). Importantly, after pontine transection the respiratory modulation of tSN activity was greatly reduced [6]. In all cases, however, the sympathetic baroreflex-induced lowering of tSN persisted and the barostimulation shortened the apneustic inspiratory burst (see Fig. 143.2A4).

Figure 143.2B1–B4 shows the results of our simulation of the effects of transient barostimulation during different phases of the respiratory cycle using the computational model described above (Fig. 143.1A) before (Fig. 143.2B1–B3) and after (Fig. 143.2B4) removal of the pontine compartment. The model generates a normal three-phase respiratory pattern with augmenting PN bursts (Fig. 143.2A1–A3). The sympathetic output in the model (tSN) exhibits a positive inspiratory modulation provided by the pontine IE population to RVLM and a negative post-inspiratory modulation resulting from the inhibitory inputs from the post-I population of BötC to the RVLM. Transient barostimulation applied to the barosensitive 2nd order NTS population produces a temporal reduction of tSN output via direct activation of the CVLM population that inhibits the activity of RVLM population. Stimulus application during inspiration (Fig. 143.2B1) does not affect respiratory (PN) activity. In contrast, stimuli applied during post-inspiration (Fig. 143.2B2) and late expiration (Fig. 143.2B3) prolong expiration via activation of post-I neurons of BötC that inhibit both the aug-E population and the RVLM. These interactions represent a second component of the sympathetic baroreflex involving interactions between the respiratory and sympathetic circuits. Similar to our experimental data (Fig. 143.2A2,A3), stimulation-evoked prolongation of expiration is greater if stimulation is applied later during the expiratory phase (Fig. 143.2B2,B3).

Removing the pontine compartment in the model converts the normal eupnea-like respiratory pattern to the apneustic pattern characterized by prolonged PN busts (see Fig. 143.2B4). As demonstrated previously [2], this pattern is characterized by a lack of post-I activity that is strongly dependent on pontine drive. Therefore, with the pons removed, the respiratory modulation of tSN (formed by inputs from pontine IE and BötC's post-I populations to RVLM) is abolished. Simultaneously, the central suppression of the baroreflex gain by the rVRG early-I(2) population, whose activity in the model is also dependent on the pontine drive, is eliminated with pontine removal. Therefore the applied barostimulation can activate post-I population during inspiration and produce an advanced termination of the apneustic inspiratory bursts hence shortening inspiration (compare Fig. 143.2B4 with Fig. 143.2A4).

Figure 143.2B5 illustrates the neural mechanism by which the transient barostimulation applied during expiration prolongs this expiration in the intact model (see Fig. 143.2B3 for comparison). The post-I neurons of BötC when activated inhibit all inspiratory (and aug-E) neurons and initiate the post-inspiratory phase of expiration. During expiration, the activities of these neurons decrement hence releasing aug-E neurons form inhibition and allowing for their gradual activation (see unperturbed breathing cycles in Fig. 143.2B5). When a barostimulus occurs during expiration, the post-I population is activated and inhibits the aug-E population, hence producing a "resetting of expiration". This resetting of expiration by the transient barostimulation provides a mechanistic explanation for expiratory period prolongation. To test this model prediction, extracellular recordings of post-I and aug-E neurons were made within the BötC of *in situ* rat preparations [4] (see example in Fig. 143.2A5). With the transient increase in perfusion pressure during expiration, the activity of post-I neurons increased and the activity of aug-E neurons decreased in full accordance with the model prediction (compare Fig. 143.2A5 with Fig. 143.2B5). In most cases,

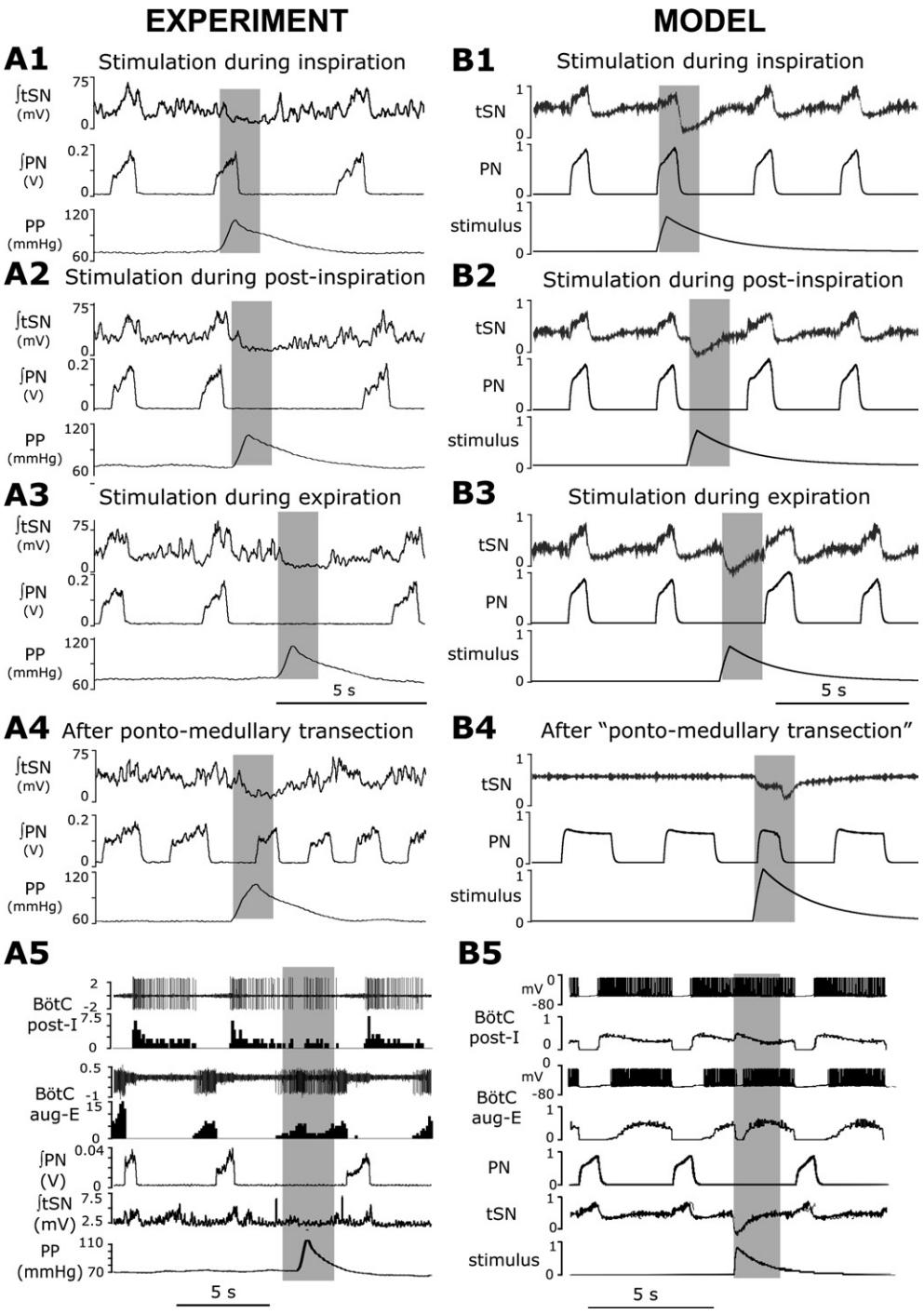


**FIGURE 143.2** Effects of transient, respiratory phase-dependent baroreceptor stimulation on phrenic (PN) and sympathetic (tSN) nerve activities *in situ* and in the model. (A1–A5) Experimental results from the arterially perfused in situ preparation A1-A3: Stimulation was applied to the intact preparation during inspiration (A1), post-inspiration (A2) and late expiration (A3). After pontine transection (A4), the applied stimulus shortened the apneustic inspiratory (PN) burst. Traces from top to bottom: integrated sympathetic (tSN) activity, integrated phrenic (PN) activity; perfusion pressure (PP). In A5, top two traces show an extracellular recording from a post-I neuron in BötC and the histogram of its activity; the next pair of traces show a simultaneous extracellular recording from an aug-E neuron of BötC and the corresponding histogram; the remaining traces show the integrated activities of PN and tSN) and perfusion pressure (PP). (B1–B5) Corresponding simulation results. In simulations shown, the stimulus was applied during inspiration (B1), post-inspiration (B2) and late expiration (B3), and also after removal of the pontine compartment in the model (B4). In B5, the top pair of traces show membrane potential of a randomly chosen neuron from the post-I population of BötC and integrated spike histogram of the entire post-I population. Second pair of traces: membrane potential of a randomly chosen neuron from the aug-E population of BötC and spike histogram of the entire aug-E population.

the barostimulation applied during expiration resulted in prolongation of expiration, and this prolongation was greater when stimulation was applied later in expiration.

These studies have clarified the role of baroreceptor input in activating post-I neurons and inhibiting aug-E neurons and demonstrated that even weak excitatory input from baroreceptors to the post-I neurons can account for the prolongation of expiration and the corresponding effect on tSN activity. In general, this demonstrates an important contribution of central sympatho-respiratory interactions to the baroreceptor control of arterial pressure.

## SYMPATHETIC NERVE ACTIVITY FOLLOWING CHRONIC INTERMITTENT HYPOXIA-INDUCED SENSITIZATION OF CENTRAL CHEMORECEPTORS

Recurrent episodes of hypoxia, such as observed in obstructive sleep apnea lead to the development of hypertension. It was shown that rats exposed to chronic intermittent hypoxia (CIH) exhibited higher levels of arterial pressure associated with an elevated sympathetic vasomotor tone [7,8] and an enhanced respiratory modulation

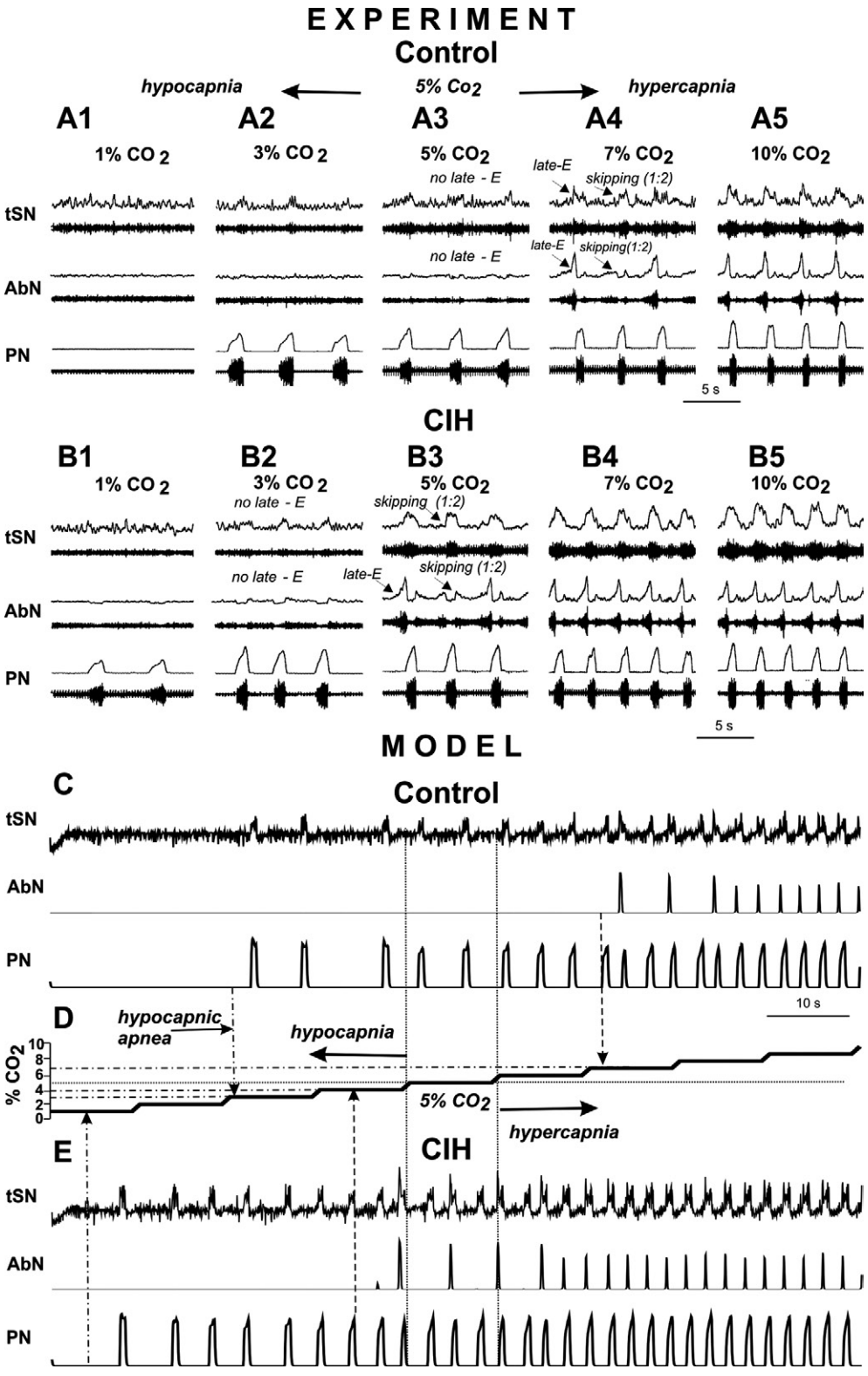


**FIGURE 143.3** Sympathetic and respiratory responses to hypercapnia before and after CIH-conditioning: experimental records and simulations. (A1–A5) Activity of phrenic (PN), abdominal (AbN), and thoracic sympathetic (tSN) nerves in the representative control preparation at 5% $CO_2$ (base level, A3), during hypercapnia (7% $CO_2$ in A4 and 10% $CO_2$ in A5) and during hypocapnia (3% $CO_2$ in A2 and 1% $CO_2$ in A1). Note the skipping of some late-E bursts in both AbN and tSN at 7% $CO_2$ (in A4). (B1–B5) PN, AbN, and tSN activities in the representative CIH-conditioned preparation at 5% $CO_2$ (base level, B3), during hypercapnia (7% $CO_2$ in B2 and 10% $CO_2$ in B3) and hypocapnia (3% $CO_2$ in B2 and 1% $CO_2$ in B1). Note the presence of late-E bursts in both AbN and tSN at 5% $CO_2$ (in B1). The activity of each nerve is represented by raw recording (bottom trace) and integrated activity (upper trace). (C–E) Model performance in simulated control (C) and CIH (E) cases. In both cases, integrated activity for phrenic (PN), abdominal (AbN) and thoracic sympathetic (tSN) outputs are shown. The $CO_2$ level was changed in a step-wise manner from 1% (hypocapnia) to 10% (hypercapnia) which is shown in panel D. The dashed vertical arrows indicate $CO_2$ levels for emerging late-E activity and for hypocapnic apnea, respectively.

of sympathetic activity [7]. This suggests that central coupling between respiratory and sympathetic circuits may contribute to hypertension in CIH-conditioned animals [8].

Typical patterns of respiratory (PN and AbN) and sympathetic (tSN) activities in the naïve rat (arterially perfused *in situ* preparation) are shown in Fig. 143.3A1–A5. Under normal conditions (5% $CO_2$), the integrated PN burst has an augmenting profile, AbN shows low-amplitude activity, and the tSN expresses an augmenting inspiratory modulation (Fig. 143.3A3). Hypercapnia (increase in $CO_2$ level from 5%) evokes high-amplitude late-expiratory (late-E) AbN discharges, which are phase-locked

to PN bursts (Fig. 143.3A4,A5; see also [3,5]). With progressive development of hypercapnia, the ratio of AbN late-E burst frequency to PN burst frequency quantally (step-wise) increases from about 1:4/1:3 to 1:2 (at 7% $CO_2$), when approximately each second respiratory cycle was skipping in AbN late-E activity (Fig. 143.3A4), and finally, to 1:1 as the $CO_2$ level increases to 10% (Fig. 143.3A5), when the AbN late-E discharges preceding PN bursts are observed in every respiratory cycle [3]. This $CO_2$-induced AbN late-E activity appears to originate in the RTN/pFRG region [3,5,9] that is also known to be a major site for central chemoreception [10]. The $CO_2$-censitive RTN/pFRG neurons project to both VRC and RVLM. The latter is important for the sympatho-excitation and the corresponding increase of arterial pressure observed during hypercapnia. The hypercapnia-evoked late-E activity, quantally accelerated with an increase in $CO_2$, has been observed in tSN (Fig. 143.3A4,A5). Moreover, the tSN late-E activity coincides with the AbN late-E bursts, suggesting a common source of late-E activities in AbN and tSN located the RTN/pFRG.

The interesting effect of CIH conditioning is that it alters the AbN and tSN activities in both normocapnia and hypercapnia [7,8]. Figure 143.3B3 shows that the juvenile rats submitted to CIH for 10 days exhibits an expressed late-E activity in both AbN and tSN (with a frequency ratio to PN of about 1:3/1:2) in the baseline conditions (5% $CO_2$), and at 7% $CO_2$ this ratio already reaches 1:1, i.e. full synchronization (Fig. 143.3B4). We suggest that CIH conditioning augment the $CO_2$ sensitivity of RTN/pFRG neurons, and hence reduces $CO_2$ threshold for the emergence of late-E oscillations seen in both AbN and tSN.

The computational model shown in Figure 143.1A was used for simulating the effect of CIH-induced sensitization of RTN/pFRG neurons on the respiratory and sympathetic activities and the sympatho-respiratory response to hyper- and hypocapnic conditions. The model includes excitatory tonic drives from several sources including RTN/pFRG that is considered to be a major central chemoreceptor site sensitive to $CO_2$ [10]. In the model, we consider RTN/pFRG tonic drive to be not constant but dependent on the $CO_2$ level as shown in Figure 143.1C (solid curve). As hypothesized above, the $CO_2$ sensitivity of RTN/pFRG increases as a result of CIH exposure. This is simulated by the horizontal shift of the $CO_2$-dependent RTN drive by 2% $CO_2$ to the direction of lower $CO_2$ values (to the left, see dashed curve in the Fig. 143.1C).

Figure 143.3C shows the results of our simulations with $CO_2$ step-wise increasing from 1% $CO_2$ (hypocapnia) through 5% $CO_2$ (normocapnia) to 10 % $CO_2$ (hypercapnia) as illustrated in Figure 143.3D. In our simulations, progressive hypercapnia (Fig. 143.3C,D, right part of the graph) leaded to the emergence and quantal acceleration of late-E bursts in both AbN and tSN, which was consistent with experimental records (see panels A3–A5). Specifically, the late-E discharges in AbN and tSN appeared at 7% $CO_2$ and reached 1:1 ratio to the PN bursts at 9% $CO_2$. Note also (see Fig. 143.3C,D, left part) that a reduction of $CO_2$ below 3% caused "hypocapnic apnea" (a lack of PN activity).

To simulate CIH conditions, the curve reflecting the $CO_2$ dependence of RTN/pFRG drive was shifted to the left (Fig. 143.1C). As a result of this shifting, the late-E bursts in AbN and tSN emerged at 4% $CO_2$, and in the normocapnic state (5% $CO_2$) they showed a stable 1:2 ratio to the PN bursts (Fig. 143.3E); at 7% $CO_2$ this ratio reached 1:1 (Fig. 143.3B4), which was consistent with our experimental observations (see Fig. 143.3B).

The second observation from the above simulation is that "CIH conditioning" reduced the apneic threshold for hypocapnia by at least 2% $CO_2$, since the PN bursts were still generated even at 1% $CO_2$ (see Fig. 143.3E, left). To check this modeling prediction, the control (naïve) and CIH-conditioned rat preparations were exposed to progressive hypocapnia (from normal 5% $CO_2$ to 3% and then to 1%). The naïve rat preparations exhibited a reduction in the integrated PN burst amplitude at 3% $CO_2$ and a hypocapnic apnea at 1% $CO_2$ (Fig. 143.3A2,A1). Importantly, these preparations never expressed late-E activity in AbN or tSN in either normocapnia or hypocapnia, and the respiratory modulation of tSN was reduced at 3% $CO_2$ and absent at 1% during hypocapnic apnea (Fig. 143.3B2,B1). In CIH rat preparations, the expressed late-E activity in both AbN and tSN was already present during normocapnia (at 5% $CO_2$) and disappeared from both nerves at 3% $CO_2$ (Fig. 143.3B2). At the same time, PN activity with a reduced amplitude (and respiratory modulation of tSN) was still present even at 1% $CO_2$ (Fig. 143.3B1), hence confirming modeling prediction on a reduction of apneic threshold for hypocapnia in CIH-conditioned rats.

Our multidisciplinary investigation suggests that the arterial blood pressure elevation associated with CIH may result from an increased $CO_2$ sensitivity of central chemoreceptors and early emergence of late-E oscillations in the RTN/pFRG.

## References

[1] Alheid GF, McCrimmon DR. The chemical neuroanatomy of breathing. Respir Physiol Neurobiol 2008;164:3–11.

[2] Smith JC, Abdala APL, Koizumi H, Rybak IA, Paton JFR. Spatial and functional architecture of the mammalian brain stem respiratory network: a hierarchy of three oscillatory mechanisms. J Neurophysiol 2007;98:3370–87.

[3] Molkov YI, Abdala APL, Bacak BJ, Smith JC, Paton JFR, Rybak IA. Late-expiratory activity: Emergence and interactions with the respiratory CPG. J Neurophysiol 2010;104:2713–29.

[4] Baekey DM, Molkov YI, Paton JFR, Rybak IA, Dick TE. Effect of baroreceptor stimulation on the respiratory pattern: Insights into respiratory-sympathetic interactions. Respir Physiol Neurobiol 2010;174:135–45.

[5] Abdala APL, Rybak IA, Smith JC, Paton JFR. Abdominal expiratory activity in the rat brainstem-spinal cord in situ: Patterns, origins and implications for respiratory rhythm generation. J Physiol 2009;587:3539–59.

[6] Baekey DM, Dick TE, Paton JFR. Pontomedullary transection attenuates central respiratory modulation of sympathetic discharge, heart rate and the baroreceptor reflex in the in situ rat preparation. Exp Physiol 2008;93:803–16.

[7] Zoccal DB, Simms AE, Bonagamba LG, Braga VA, Pickering AE, Paton JFR, Machado BH. Increased sympathetic outflow in juvenile rats submitted to chronic intermittent hypoxia correlates with enhanced expiratory activity. J Physiol 2008;586:3253–65.

[8] Zoccal DB, Paton JFR, Machado BH. Do changes in the coupling between respiratory and sympathetic activities contribute to neurogenic hypertension?. Clin Exp Pharmacol Physiol 2009;36:1188–96.

[9] Janczewski WA, Onimaru H, Homma I, Feldman JL. Opioid-resistant respiratory pathway from the preinspiratory neurones to abdominal muscles: In vivo and in vitro study in the newborn rat. J Physiol 2002;545:1017–26.

[10] Guyenet PG, Stornetta RL, Bayliss DA. Retrotrapezoid nucleus and central chemoreception. J Physiol 2008;586:2043–8.